Journal of Digital Imaging

Extraction of Metastatic Lymph Nodes from MR Images Using Two Deformable Model-based Approaches

Jia-Yin Zhou,[1] Wen Fang,[2] Kap-Luk Chan,[1,2] Vincent F. H. Chong,[3] and James B. K. Khoo[4]

We presented and evaluated two deformable model-based approaches, region plus contour deformation (RPCD), and level sets to extract metastatic cervical nodal lesions from pretreatment T2-weighted magnetic resonance images. The RPCD method first uses a region deformation to achieve a rough boundary of the target node from a manually drawn initial contour, based on signal statistics. After that, an active contour deformation is employed to drive the rough boundary to the real node–normal tissue interface. Differently, the level sets move a manually drawn initial contour toward the desired nodal boundary under the control of the evolvement speed function, which is influenced by image gradient force. The two methods were tested by extracting 33 metastatic cervical nodes from 18 nasopharyngeal carcinoma patients. Experiments on a basis of pixel matching to reference standard showed that RPCD and level sets achieved averaged percentage matching at 82–84% and 87–88%, respectively. In addition, both methods had significantly lower interoperator variances than the manual tracing method. It was suggested these two methods could be useful tools for the evaluation of metastatic nodal volume as an indicator of classification and treatment response, or be alternatives for the delineation of metastatic nodal lesions in radiation treatment planning.

KEY WORDS: Object extraction, magnetic resonance imaging, deformable model, level sets, nasopharyngeal carcinoma, metastatic cervical nodes

INTRODUCTION

Regional lymphatic metastasis is very common in patients with head and neck squamous cell carcinomas (HNSCC). Some HNSCC, such as nasopharyngeal carcinoma (NPC), have a high degree of regional spread at presentation, although the primary tumor may have the appearance of a small or early lesion.[1] Neck nodes are currently radiologically N-classified by largest transverse diameter, the number of nodes, and unilateral or bilateral involvement.[2] Recent studies suggest that metastatic nodal volume be an important prognostic factor in the treatment of HNSCC.[3–5] Therefore, it is important to accurately delineate lymph node boundary, in computer tomography (CT) or magnetic resonance (MR) images, to measure the nodal volume for the purposes of prognosis and monitoring treatment response over time. In addition, accurate delineation of metastatic nodal lesions is also a crucial issue in the treatment planning of neck irradiation, especially in the application of intensity modulated radiation therapy where tight margins around the lesions can be prescribed with highly conformed pattern of dose distribution.

Nowadays, the contouring of metastatic lymph nodes is still manually done in medical practice by diagnostic radiologist or radiation oncologist

[1]*From the School of Chemical and Biomedical Engineering, Nanyang Technological University, Singapore, Singapore.*

[2]*From the School of Electrical and Electronic Engineering, Nanyang Technological University, Singapore, Singapore.*

[3]*From the Department of Diagnostic Radiology, National University of Singapore, Singapore, Singapore.*

[4]*From the Department of Oncologic Imaging, National Cancer Centre, Singapore, Singapore.*

Correspondence to: Jia-Yin Zhou, Biomedical Engineering Research Centre, Nanyang Technological University, 50 Nanyang Avenue, Singapore, Singapore 639798; tel: +65-67906421; fax: +65-67912274; e-mail: zhoujy@pmail.ntu.edu.sg

Online publication 5 January 2007
doi: 10.1007/s10278-006-1037-2

using a set of axial diagnostic CT/MR images or planning CT images. Most studies on head and neck tumor or nodal volume are CT-based, where volume measurements are determined by summation-of-area technique. It is a tedious, labor- and time-consuming procedure with considerable intra- and interoperator variance (IV), and the accuracy of the manual contouring may highly depend on the operator's experience. Honea et al.[6] reported the use of active contours to segment lymph nodes from CT images. The contour initialization and search strategy were improved for better performance, but the results could still be affected by local image gradients and artifacts. Teng et al.[7] developed a method for automatically selecting and adapting standardized regions of cervical lymph nodes and microscopic spread of disease, together with CT image registration. To our knowledge, there is still no study on computerized lesion delineation for metastatic lymph nodes based on MR imaging. In addition, several separated nodal lesions (multiple cervical nodes with bilateral involvement) may exist in the same image, which traditional object extraction methods cannot handle within one single procedure.

In this paper, we present two deformable model-based approaches, region plus contour deformation (RPCD) and level sets, for the extraction of metastatic cervical nodal lesions from pretreatment coronal T2-weighted (T2W) MR images. The extraction accuracies and interoperator reliabilities of the two methods were also evaluated using MR images from 18 NPC patients, with the comparison to the reference standard (RS) drawn by an experienced radiologist. The development of robust nodal extraction techniques is aimed at providing an efficient and consistent way for nodal classification and quantitative assessment of treatment response, as well as providing a useful tool to facilitate future automatic treatment planning system, with the fusion of CT/MR images.

The remainder of the paper is organized as follows: The mathematic fundamentals of RPCD and level sets methods are described in the "OBJECT EXTRACTION METHODS" section. Data acquisition, experiments and data processing are introduced in the "DATA AND PROCESSING" section, followed by the "RESULTS" section. Finally, we discuss the algorithms with achieved results and give conclusions.

OBJECT EXTRACTION METHODS

RPCD

The RPCD method is an improvement of the active contour model,[8] with a region deformation procedure in advance. For classic active contour model, edge information (gradient) and contour smoothness are used to drive a contour for object boundary location. However, the high gray level gradient of the image may be because of object boundary as well as noise and object texture, and therefore the optimization functions may have many local optima. Consequently, the initial contour is required to be "close enough" to the real boundary. One solution is to use a region deformation before the contour deformation (active contour model), as region information provides more regional constraints on the boundary and the region model can tolerate certain noise and textures.[9]

An object can be regarded as a region that is homogeneous in some properties and its boundary can be considered as a subregion of the object that borders other objects. The property with some disparities between an object and its surrounding area should be chosen to identify the object. The goal of region deformation is to find a region of maximum area whose boundary has the same properties as the region, based on an initial estimation of the object. Therefore, a property disparity between a region and its boundary, and the area information of the region can be used to make the judgment.[9] In this study, the grayscale statistical distribution of fat suppressed T2W MR images was chosen as the discrimination parameter as the lymph node has a high contrast to the surrounding tissues such as muscles and fat.

Let I be the pixel set of an image, $i \in I$ be a pixel; g_i is the grayscale of i with $0 \leq g_i \leq 255$. An object in the image can be described as a homogenous region O, and the boundary of O is a simple closed curve B. As the nonparametric Kolmogorov–Smirnov (KS) test can test if two sets of probability distribution belong to the same particular probability distribution, it was used in this study to test whether the boundary pixel set and the object pixel set have the same grayscale distribution. The KS distances D is defined as

$$D = Max|F_B(g_i) - F_O(g_i)|, \qquad (1)$$

where F_B and F_O are the grayscale cumulative frequency distribution functions of B and O, respectively. A lower case d, which depends on the pixel numbers of B and O, is defined as

$$d = c \Big/ \sqrt{AL/(A+L)}, \tag{2}$$

where c is the test significance level, A is the number of pixels form O, and L is the number of pixels form B. The hypothesis F_B=F_O is only accepted when $D \leq d$.

After putting an initial contour and calculating the KS test using Eqs. 1 and 2, two morphological operations are used to deform the region for the final converge of the region to meet F_B=F_O, based on the different results of the KS test. If $D>d$, the region plan covers a region somewhat different from the desired object and a shrinking operation is used to deform the region by shrinking the current contour inward for one pixel. However, not all boundary elements need shrink inward, but only those that have a different property within the region. Figure 1 shows how to determine which boundary elements should be deleted. Here, O is the object, B is its boundary, and j is a pixel of B. A small window W_j is set with j being the center. If the grayscale distribution of W_j is close to that of O, j is kept; otherwise it is deleted. The shrinking operation is performed till $D<d$. When $D<d$, the region plan may exactly cover the actual object or may be completely inside the object and not cover the whole object. Because of this kind of possibility, a growing operation is performed such that the current contour will grow outward for one pixel till $D>d$. In the implementation, an initial contour was put totally inside or outside the actual object, or to partly cover the actual object, and the KS test was performed. There might be two results: (1) If initially $D>d$, the shrinking operation was performed till $D<d$. Then a cycle of growing operation was performed. After an iteration containing one growing operation and one shrinking operation, the new region area was compared with the previous one. The process stopped if the region area did not change. (2) If initially $D<d$, the growing operation was performed till $D>d$ following the steps as described in (1).

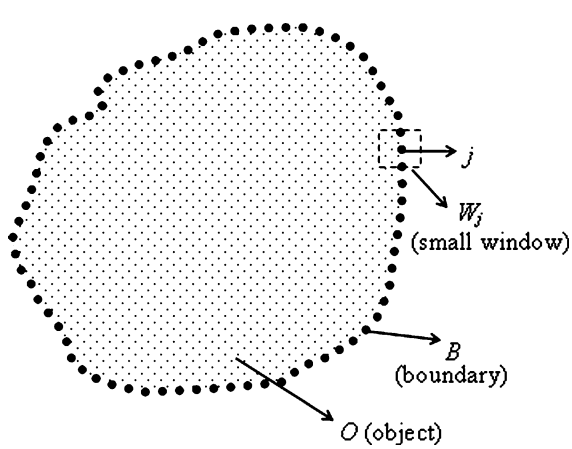

Fig 1. Object described as a region with a closed curve as its boundary.

The extracted boundary after region deformation is a rough contour of the real object boundary as the region deformation ignores the actual object boundary and smoothness but keeps the local shape constraint of the object from the statistics measure of the whole object. Hence, the extracted boundary is locally different from the real boundary and it is further refined by the contour deformation using a fast snake (active contour) method.[10]

Level Sets

Also, as a geometric deformable model, the level sets embed the initial position of a curve as the zero level set of a higher dimensional function. Then, instead of moving the curve, the hypersurface function is moved to expand, shrink, rise, and fall to track the motion of the curve, driven by its speed function correlated with the image gradient force.[11,12] In addition, level sets have the ability to extract shapes in concave regions and with changes in topology. The principle of level sets can be described as below:

Let $C(\mathbf{p},t)$, defined as $\{x(\mathbf{p},t), y(\mathbf{p},t)\}$, denote a family of closed contours generated by moving an initial contour $C_0(\mathbf{p})$ in the direction of its Euclidean normal inward vector $\mathbf{N}$,[13] as shown in Figure 2. Assuming the speed of the curve movement is a scalar function F of the contour curvature K, the evolution equation can be written as

$$\begin{cases} C_t(\mathbf{p},t) = F(K)\mathbf{N} \\ C(\mathbf{p},0) = C_0(\mathbf{p}). \end{cases} \tag{3}$$

To solve the above evolution equation, the level set method represents the contour $C(\mathbf{p},t)$ implicitly as the zero level set of a smooth, continuous scalar

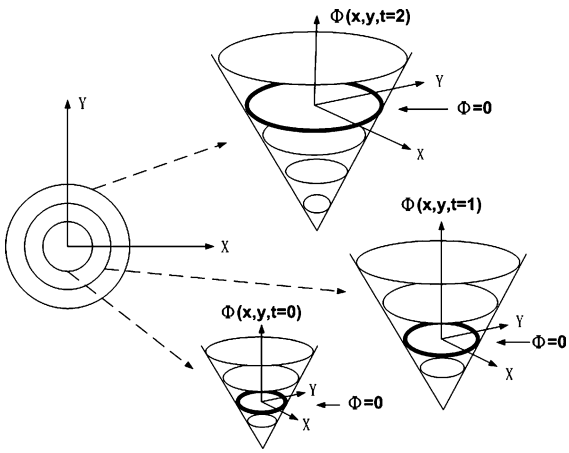

Fig 2. An illustrator of level sets.

function, known as *level set function*, where $x,y \in R^2$.[14] This implicit contour at any time t is given by $C(\mathbf{p}, t) = \{x, y | \Phi(x, y, t) = 0\}$.

Taking derivation of $\Phi(x,y,t)=0$ with respect to time and space, the following partial differential equation can be derived from Eq. 3

$$\begin{cases} \Phi_t = -F(K)|\nabla\Phi| \\ \Phi(C_0(\mathbf{p}), 0) = 0 \ , \end{cases} \tag{4}$$

where ∇ is the gradient operator and $|\nabla\Phi|$ denotes the gradient norm. Thus, a connection is established between the family of the moving curves $C(\mathbf{p},t)$ and the family of evolving level set surfaces $\Phi(x,y,t)$.

To use the level sets to detect object in images, the speed function $F(K)$ should be multiplied with stopping criteria to make the level sets stop evolving when the contour is approaching near the actual object boundary. This stopping criteria are usually defined as

$$k_I(x, y) = \exp(-E_I(x, y)), \tag{5}$$

where $E_I(x, y) = \left|\nabla G_\sigma^* I(x, y)\right|$ is defined as the gradient of a Gaussian filter convoluted with the image I. For the original speed function with the form $F(K) = C - \varepsilon K$, the new one after multiplication is expressed as

$$F = (C - \varepsilon K) \cdot \exp(-E_I), \tag{6}$$

where C is an image-dependent balloon force added to control the contour to flow inward (or outward) and ε is a positive constant term as the weight. In the implementation, C is often set to be +1 or −1, hence the speed function F is a function of contour curvature K as well as the image gradient. When the contour is close to the actual object boundary, the speed function will be close to 0, resulting in the stop of the evolution process.

DATA AND PROCESSING

MR Images for Testing

This study, approved by the Ethics Committee, included 149 coronal T2W fat-suppressed MR images (fast spin echo sequence; repetition time range 4,000–5,800 ms; echo time range 85.3–94.1 ms; image size 256×256 pixels; field of view 210–240 mm; and slice thickness 5 mm without gap), from 18 histologically confirmed adult NPC patients who had MR imaging (1.5 T scanner, Signa, GE Medical Systems, Milwaukee, WI, USA) performed for staging before radiation therapy.

Experiments

Two head and neck radiologists (operator 1, 14 years of experience; operator 2, 10 years of experience) independently performed the manual tracing task in coronal T2W images for nodal lesions, using a graphic user interface developed by this group on a PC work station. The radiologists could, however, refer to images of other planes or sequences acquired in the imaging protocol to aid in the accurate delineation of lymph nodes. Both of them followed a common protocol: For each patient, the cervical and retropharyngeal lymph nodes whose axial largest diameters are more than 1.0 cm were selected for measurement; If two or more nodes are in contact with each other, the entire mass is considered as one node for the purpose of delineation; However, enlarged retropharyngeal nodes that cannot be separated from primary tumors were excluded. According to this protocol, two Ph.D. students independently performed computerized extraction using both RPCD and level sets algorithms, by giving initial contours. For images with several lesions in the same lateral, each node needed an individual initial contour when using deformable RPCD, whereas only one contour was needed when using level sets. All extraction results were recorded for analysis.

Evaluation Data Analysis

Algorithm evaluation was performed at pixel level for extraction accuracy and interoperator reliability.

Extraction accuracy: The "RS" of metastatic nodal lesions, against which computerized extraction results could be compared, was from the manual tracing results done by operator 1. The following were calculated: true positives (TPs, RS pixels found algorithmically), false positives (FPs, pixels isolated as lesion but not within RS), and false negatives (RS pixels not found algorithmically). Two measures, percentage matching (PM)[15] and Jaccard measure (JM), were calculated as follows:

$$\mathrm{PM} = \frac{\mathrm{TPs}}{\mathrm{RS}} \times 100\%, \tag{7}$$

$$\mathrm{JM} = \frac{\mathrm{TPs}}{\mathrm{RS} + \mathrm{FPs}}. \tag{8}$$

An ideal PM value is 100% while a value of 0 indicated that there is a complete miss. Considering the importance of FPs, the JM compares the isolated lesion with the summation of RS and FPs in size and location.

Interoperator reliability: IV shown in Eq. 9 was used to estimate the interoperator reliabilities of manual tracing and two computerized extraction algorithms.

$$\mathrm{IV}_X = 1 - \frac{\mathrm{A}_{X1} \cap \mathrm{A}_{X2}}{\mathrm{A}_{X1} \cup \mathrm{A}_{X2}} \times 100\% \tag{9}$$

where IV_X is for IV of method X (manual tracing, RPCD, or level sets), A_{X1} is extracted or traced nodal mass obtained by operator 1 and A_{X2} is that obtained by operator 2 on the same image; $A_{X1} \cap A_{X2}$ is the overlap of A_{X1} and A_{X2} while $A_{X1} \cup A_{X2}$ is the merging of A_{X1} and A_{X2}. A value of 0 shows the perfect reliability while a value of 1 shows no reliability.

In the implementation, lesion regions identified by means of computerized extraction were compared with RS at the pixel level on a per slice basis, whereas the comparisons of PM, JM, and IV values between methods or operators were based on total volume of per lymph node or lymph node mass. The nonparametric Friedman's test was used to evaluate the (1) differences in both PM and JM between the two computerized extraction methods, and (2) interoperator variations of both PM and JM between the two operators of computerized extraction. Moreover, we compared IVs from the various methods by means of multiple Wilcoxon rank-sum tests. All statistical results were calculated using Matlab 6.5 (The MathWorks Inc., Natick, MA, USA). Differ-

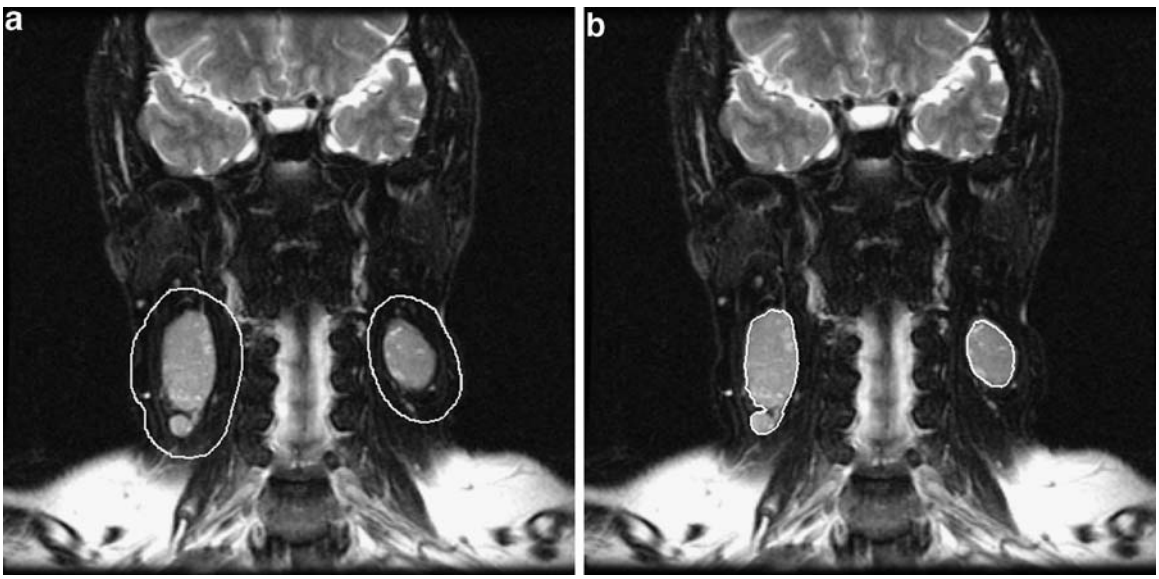

Fig 3. The extraction of nodal lesions using RPCD. (a) The two initial contours and (b) final results.

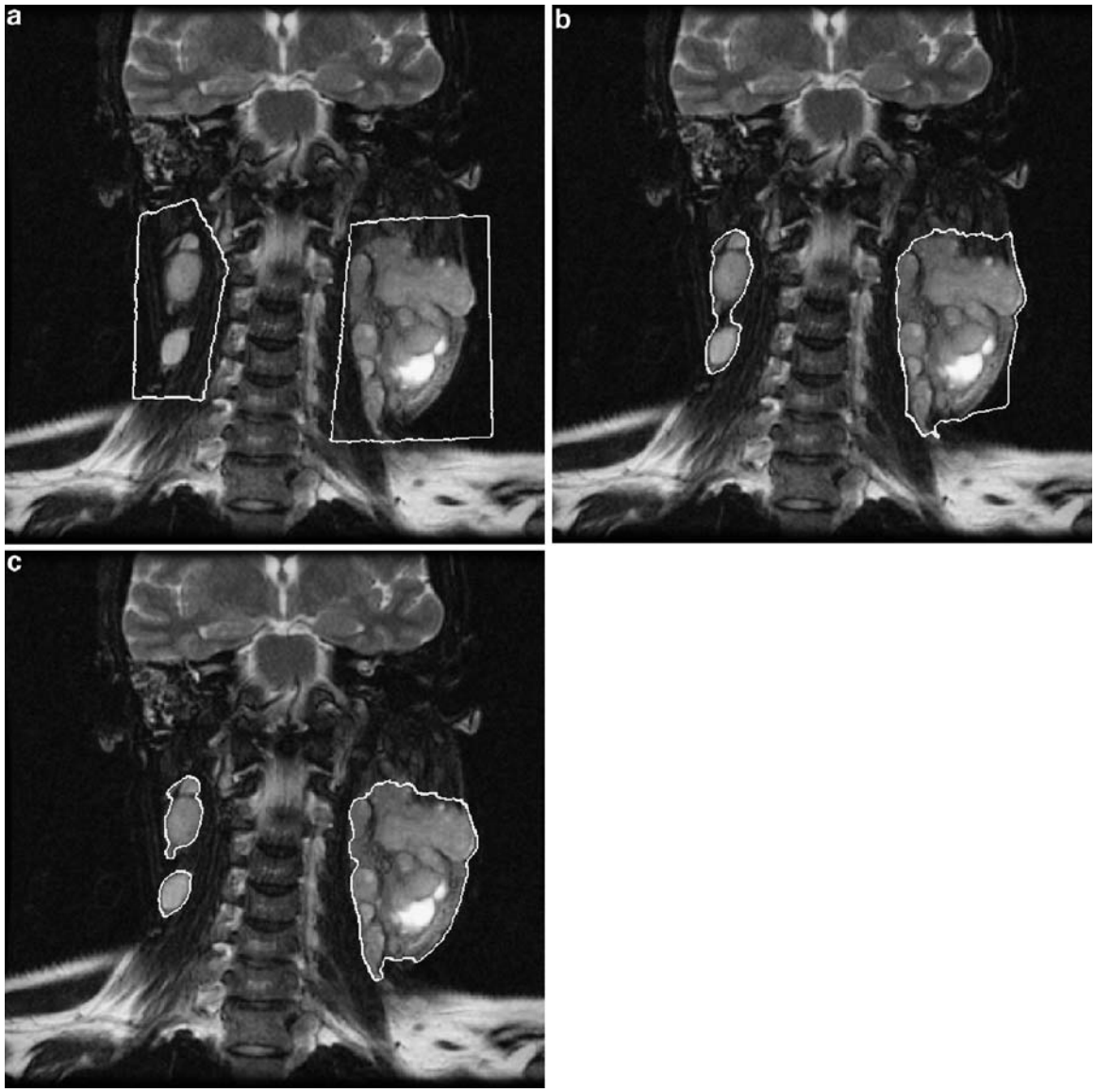

Fig 4. The extraction of nodal lesions using level sets. (a) The initial contours, (b) the evolution of level sets, note the split of contour on the right lateral, and (c) final results.

Table 1. Percentage Matching and Correspondence Ratio Comparing Reference Standard and Computerized Extractions

	PM_{R1} %	PM_{R2} %	PM_{L1} %	PM_{L2} %	JM_{R1}	JM_{R2}	JM_{L1}	JM_{L2}
Minimum	63.52	72.33	58.54	57.35	0.48	0.50	0.52	0.50
Maximum	92.41	91.61	96.95	95.87	0.88	0.90	0.86	0.85
Mean±SD	82.83±5.78	84.51±4.31	88.04±9.85	87.10±10.31	0.77±0.08	0.79±0.08	0.72±0.09	0.72±0.09

PM_{RX} and PM_{LX}: the percentage matching obtained using RPCD and level sets, respectively, by operator X; JM_{RX} and JM_{LX}: the correspondence ratios obtained using RPCD and level sets, respectively, by operator X.

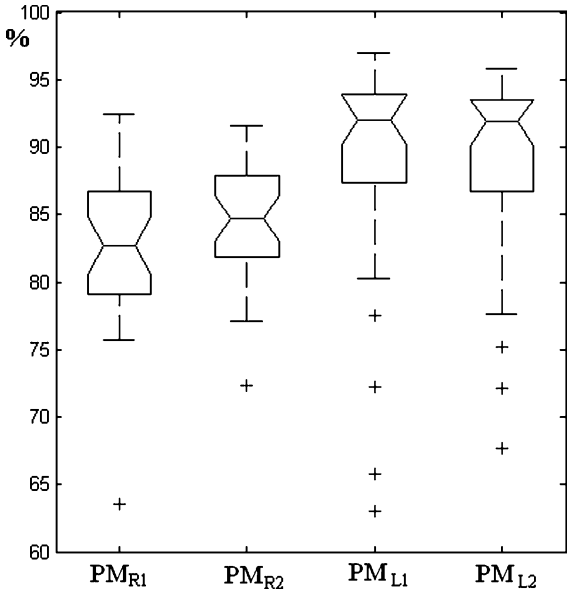

Fig 5. The distribution of percentage matching (PM) obtained using RPCD (R) and level sets (L) by two operators.

ences with $p<0.05$ were considered significant for Friedman's tests, whereas for the Wilcoxon rank-sum test, $p<0.01$ was considered to be statistically significant to correct for multiple comparisons.

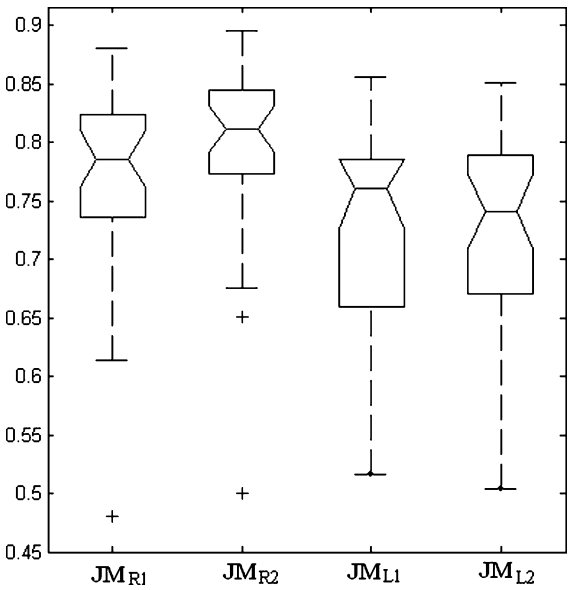

Fig 6. The distribution of Jaccard measure (JM) obtained using RPCD (R) and level sets (L) by two operators.

Table 2. Comparison of IV Among Manual Tracing and Computerized Extractions

	IV_M%	IV_R%	IV_L%
Minimum	12.12	6.56	3.23
Maximum	55.19	29.20	28.12
Mean±SD	17.08±7.58	13.39±5.90	10.37±5.64

IV_M, IV_R, and IV_L: interoperator variances of manual tracing, RPCD, and level sets, respectively.

RESULTS

RPCD and level sets methods were evaluated using 149 MR images containing 33 enlarged lymph nodes from 18 NPC patients. Examples of extraction results using RPCD and level sets are shown in Figures 3 and 4, respectively.

The computerized nodal lesion extraction evaluated by PM and JM values is presented in Table 1 and Figures 5 and 6, respectively. The Friedman's test on PM shows that level sets extracted significantly more TP areas than RPCD ($p = 1.67\times$

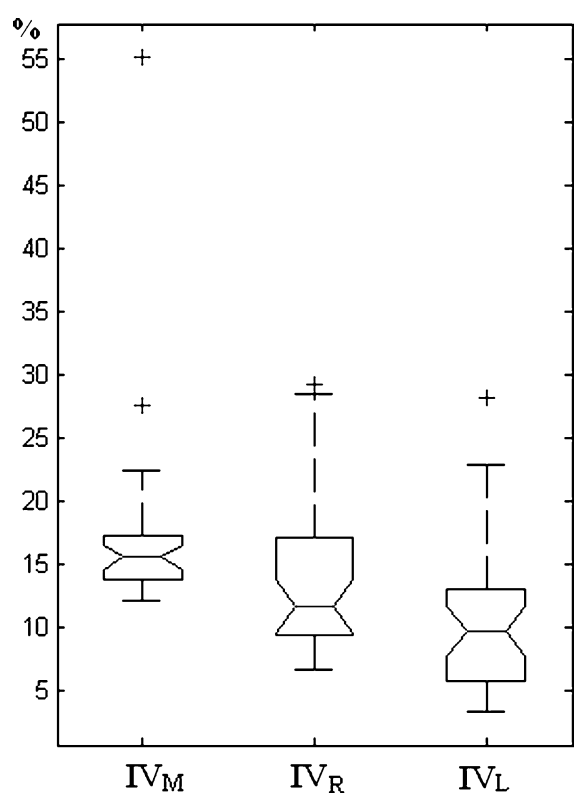

Fig 7. The distribution of interoperator variance (IV) of manual tracing (M), RPCD (R), and level sets (L).

10^{-5}), but no significant difference existed between the TP areas from two operators (p=0.727). On the other hand, JM obtained by level sets was significantly lower than that obtained using RPCD ($p = 4.46 \times 10^{-5}$), and these was also no significant difference between the JMs from two operators (p=0.362). This means that level sets also extracted much more FP regions than RPCD.

Table 2 and Figure 7 show the distribution of IVs from the various methods. The averaged IV of RPCD is significantly lower than that of manual tracing (p=0.003). Level sets also achieved significantly lower IV than manual tracing ($p = 1.836 \times 10^{-6}$). Comparing IVs from level sets with the ones from RPCD, we found that level sets obtained lower IV, but there was no statistical significance (p=0.018).

DISCUSSION

Lymph node metastasis is an important prognostic factor in the treatment of HNSCC. A single nodal metastasis, regardless of location or size of the primary tumor, may reduce the prognosis of a patient by one half.[16] Over the last few decades much effort was expanded in identifying the imaging features of tumor bearing lymph nodes,[17–19] and how these nodes could be classified and unified with the system used by surgeons.[20] Investigations in recent years have pointed out the importance of nodal volume as an additional prognostic factor.[4,5] This has stimulated an interest in the quantitative analysis of lymph nodes bearing metastases. Manual extraction of metastatic nodal lesions mainly involves the tracing of nodal outlines. Whether this process is done by a radiologist or by a technologist, there is always an important element of subjectivity in determining the nodal boundary, therefore resulting in both intra- and interoperator variations.[21] Moreover, radiation therapists also need to draw the contours of lymph nodes in axial or coronal plan for treatment planning. With the increasing adoptions of 64-slice CT systems, the burden of lesion and organ-at-risk contouring will increase

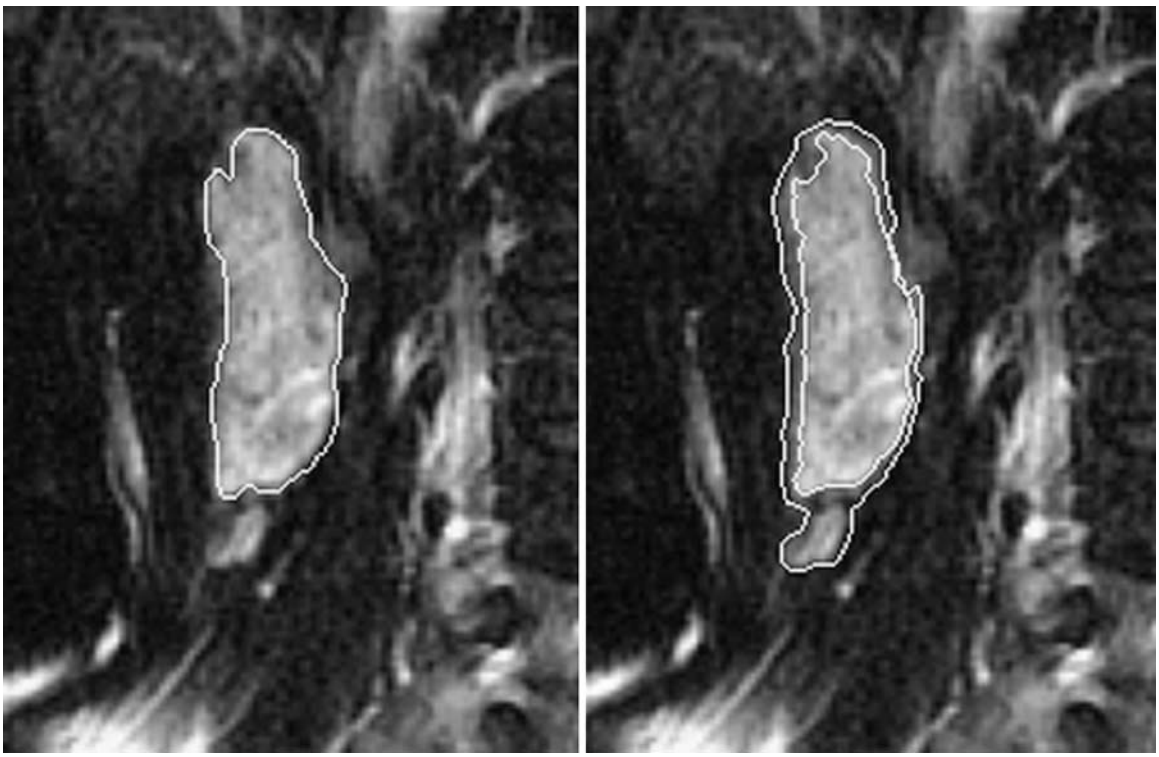

Fig 8. Magnified image of boundaries extracted using manual tracing (left), RPCD (right, inner contour), and level sets (right, outer contour) from the same lymph node. Note the distance between RPCD obtained boundary and level sets obtained boundary.

dramatically. Hence, the adoption of computerized methods for efficient lesion extraction and intra- and interoperator variation reduction is extremely important if lymph node contouring becomes an established procedure in lymph node classification, treatment planning, and the monitoring of treatment response. Currently, the focus is on the computerized segmentation of primary tumor of HNSCC whereas nodal metastasis determination is relatively neglected.

The RPCD method was implemented by a region deformation followed by a succeeding contour deformation (active contour) to locate the boundary of nodal lesions from an initial contour. The region deformation procedure is actually a constrained optimization problem in which maximizing the region area is the objective, with the region and its boundary having the same grayscale distribution as the constraint. In this procedure, the drive force of deformation is from the image statistical information, not from the edge information. In most situations, we found that a majority of the resultant contour after region deformation was located inside the lesion but within 2 pixels to the actual lesion–normal tissue interface. For a few cases, the resultant contour even got an ideal lesion boundary. Therefore, region deformation provided a good initialization for the following contour deformation and the implemented fast snake (active contour) reached its local energy minimization within a few iterations, leading to the final tight boundary. This method can eliminate the "fake" boundary caused by noise, artifacts, and other sources (for example, the adjacent vascular structures in this study), but it cannot deal with multiple lesions in one operation. The resultant averaged PM reflecting the ratio of isolated TPs to RS from 82–84% is reasonable, as the tendency of manual tracing that approximates the tumor margin with a smooth and loose curve was reported before[22,23] and was also observed in this study (Fig. 8).

By using level sets, we can extract lymph nodes with the averaged PM at 87–88% that was significantly higher than the RPCD method. On the other hand, level sets obtained much more FP regions than RPCD, leading to the low averaged JM. A nodal boundary extracted by level sets is shown in Figure 8, where a majority of the contour is several pixels but consistently outside the actual boundary. This may be explained as follows: The evolution speed of level sets contour is driven by the contour curvature and image gradient. As long as the gradient information of nodal lesions is strong enough, level sets curve can extract the desired lesions correctly. In this study, a Gaussian filter was applied before the extraction of image gradient to partially remove the noise and artifacts that may cause false detections, but it also blurred the relatively distinct interface between lymph nodes and muscle as well as the suppressed fat. Furthermore, the stopping criteria shown in Eq. 5 have an exponential operation on the image gradient. Consequently, when level sets contour approached but still did not reach the real boundary, the enhanced stopping criteria would lower the evolution speed of level sets contour and finally stop contour evolution at a certain position. Sometimes the enclosed lymph node included either part of the internal jugular vein, which is in contact with the target lesion or small lesions that are adjacent to but separated from the target lesion. Level sets, because of the overcontouring property, may not be ideal for prognosis-oriented lymph node extraction that requires accurate boundary outlining, but it may be a good choice for treatment planning as for radiation therapy; the microscopic target area, which surrounds the target lesion but shows normal signal in images, needs sterilization as well.

Some NPC patients have multiple nodal metastases on one or both laterals of the neck. Owing to the favorable advantages of level set framework, multiple lesions on one lateral can be extracted simultaneously and human intervention can be reduced. By placing an arbitrary initial contour covering all lesions in one lateral, level sets curve can separate itself into several small contours and evolve toward each lesion, as shown in Figure 4. Having this distinguishing merit, level sets could in fact handle multiple lesions on both laterals of the neck. Nevertheless, in this application the high and intermediate signal from spinal fluid, spinal cord, and vertebra at the central part of the image hampered this ability.

For a computerized lesion contouring tool to be accepted for routine clinical use, it should reasonably have reliable interoperator consistency. For this work, the IVs in the semiautomatic methods originated from manually initialized contours for deformation because different initial contours could generate different final contours. Demon-

strating significantly lower IVs in this study, both RPCD and level sets effectively reduced the level of operator dependence compared with that with manual method. For further attempts to reduce IV, either global object detection with shape prior information or automatic initial contour generation with image filtering can be considered.

In this study, fat-suppressed T2W sequence at coronal plane was selected for lesion extraction because (1) there was relatively good contrast between the intermediate signal intensity of lymph node against a background of low-signal intensity muscle and suppressed fat signals, and (2) we have observed in our patients the tendency to have many nodes strung out along the neurovascular bundle, hence, there were fewer slices to perform the lesion extraction work under such circumstance, compared with axial sections. In T2W images, both metastatic nodal tissue and central necrosis show high signal intensity. We have not attempted to exclude necrotic areas during nodal volume measurement.

CONCLUSION

The delineation of cervical nodal lesions has clinical significance in the treatment of HNSCC. Because of the inherent defects of manual outlining, reliable computerized methods for automated lymph nodes boundary extraction are desirable. Two approaches, RPCD and level sets, were presented and evaluated using clinical MR images for nodal boundary extraction. The integration of testing indicators suggested that the RPCD method could be a robust tool to extract nodal lesions for nodal volume-based disease classification while level sets could be more suitable for treatment planning-oriented nodal boundary extraction. After further development, such tools may eventually be used during clinical trials or cancer treatment, for N-staging, quantitative monitoring of metastatic node response, and treatment planning.

ACKNOWLEDGEMENTS

This study is supported by grants from the National Medical Research Council of Singapore (NMRC/0837/2004) and the Singapore Millennium Foundation Postdoctoral Award (2004-SMF-1150). Authors also thank the support from the Biomedical Engineering Research Centre, Nanyang Technological University, Singapore.

REFERENCES

1. Chong VFH, Fan YF: Detection of recurrent nasopharyngeal carcinoma: MR imaging versus CT. Radiology 202:463–470, 1997
2. Sobin LH, Wittekind C: UICC TNM Classification of Malignant Tumors, 6th edition. New York: Wiley-Liss Press, 2002
3. Chua DT, Sham JS, Kwong DL, et al.: Volumetric analysis of tumor extent in nasopharyngeal carcinoma and correlation with treatment outcome. Int J Radiat Oncol Biol Phys 39:711–719, 1997
4. Labadie RF, Yarbrough WG, Weissler MC, Pillsbury HC, Mukherji SK: Nodal volume reduction after concurrent chemo- and radiotherapy: correlation between initial CT and histopathologic findings. AJNR Am J Neuroradiol 21:310–314, 2000
5. Jakobsen J, Hansen O, Jorgensen KE, Bastholt L: Lymph node metastases from laryngeal and pharyngeal carcinomas-calculation of burden of metastasis and its impact on prognosis. Acta Oncol 37:489–493, 1998
6. Honea DM, Ge Y, Snyder WE, Hemler PF, Vining DJ: Lymph-node segmentation using active contour. SPIE Proc 3034:265–273, 1997
7. Teng CC, Austin-Seymour MM, Barker J, Kalet IJ, Shapiro LG, Whipple M: Head and neck lymph node region delineation with 3-D CT image registration. Proc AMIA Symp 767–771, 2002
8. Kass M, Witkin A, Terzopoulos D: Snakes: Active contour model. Int J Comput Vis 1:321–331, 1988
9. Chan FHY, Lam FK, Poon PWF, Zhu H, Chan KH: Object boundary location by region and contour deformation. IEE Proc Vis Image Signal Process 143:353–360, 1996
10. Williams DJ, Shah M: A fast algorithm for active contours and curvature estimation. Comput Vis Graphics Image Process Image Underst 55:14–26, 1992
11. Malladi R, Sethian J, Vemuri B: Shape modeling with front propagation: A level set approach. IEEE Trans Pattern Anal Mach Intell 17:158–175, 1995
12. Tsai A, Yezzi A Jr, Wells W, et al.: A shape-based approach to the segmentation of medical imagery using level sets. IEEE Trans Med Imag 22:137–154, 2003
13. Han X, Xu C, Prince JL: A topology preserving level set method for geometric deformable models. IEEE Trans Pattern Anal Mach Intell 25:755–768, 2003
14. Sethian J: Level Set Methods and Fast Marching Methods. Cambridge: Cambridge University Press, 1999
15. Fletcher-Heath LM, Hall LO, Goldgof DB, Murtagh FR: Automatic segmentation of nonenhancing brain tumors in magnetic resonance images. Artif Intell Med 21:43–63, 2001
16. Batsakis JG: Squamous cell carcinoma of the oral cavity and oropharynx. In: Batsakis JG eds Tumors of the Head and Neck: Clinical and Pathological Considerations, 2th edition. Baltimore: William & Wilkins, 1979, pp 240–250
17. Chong VFH, Fan YF, Khoo JBK: MRI features of cervical nodal necrosis in metastatic disease. Clin Radiol 1:103–109, 1996
18. Curtin HD, Ishwaran H, Mancuso AA, Dalley RW, Caudry DJ, McNeil BJ: Comparison of CT and MR imaging in staging of neck metastases. Radiology 207:123–130, 1998
19. Anzai Y, Brunberg JA, Lufkin RB: Imaging of nodal metastasis in the head and neck. J Magn Reson Imaging 7:774–783, 1997
20. Som PM, Curtin HD, Mancuso AA: An imaging-based

classification for the cervical nodes designed as an adjunct to recent clinically based nodal classification. Arch Otolaryngol Head Neck Surg 125:388–396, 2004

21. Clarke LP, Velthuizen RP, Camacho MA, et al.: MRI segmentation: Methods and applications. Magn Reson Imaging 13:343–368, 1995

22. Joe BN, Fukui MB, Meltzer CC, et al.: Brain tumor volume measurement: Comparison of manual and semi automated methods. Radiology 212:811–816, 1999

23. Chong VFH, Zhou JY, Khoo JBK, Huang J, Lim TK: Nasopharyngeal carcinoma tumor volume measurement. Radiology 231:914–921, 2004